Scalable One-Pot - Liquid-Phase Oligonucleotide Synthesis for Model Network Hydrogels

Guido Creusen[a,b,c], Cecilia Oluwadunsin Akintayo[a,b,c,d], Katja Schumann,[a] Andreas Walther[a,b,c,d*]

[a] A[3]BMS Lab, Institute for Macromolecular Chemistry, University of Freiburg, Stefan-Meier-Straße 31, 79104 Freiburg, Germany

[b] Freiburg Materials Research Center, University of Freiburg, Stefan-Meier-Straße 21, 79104 Freiburg, Germany

[c] Freiburg Center for Interactive Materials and Bioinspired Technologies, University of Freiburg, Georges-Köhler-Allee 105, 79110 Freiburg, Germany

[d] DFG Cluster of Excellence "Living, Adaptive and Energy-Autonomous Materials Systems" (*liv*MatS), 79110 Freiburg, Germany.

*andreas.walther@makro.uni-freiburg.de

For Table of Contents Only

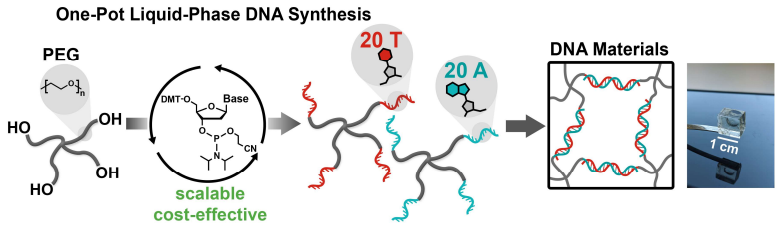

Key words: DNA hydrogels, liquid phase oligonucleotide synthesis, model networks, DNA materials, star polymers

Abstract

Solid-phase oligonucleotide synthesis (SPOS) based on phosphoramidite chemistry is currently the most widespread technique for DNA and RNA synthesis, but suffers from scalability limitations and high reagent consumption. Liquid-phase oligonucleotide synthesis (LPOS) uses soluble polymer supports and has the potential of being scalable. However, at present, LPOS requires 3 separate reaction steps and 4-5 precipitation steps per nucleotide addition. Moreover, long acid exposure times during the deprotection step degrade sequences with high A-content (adenine) due to depurination and chain cleavage. In this work, we present the first one-pot liquid-phase DNA synthesis technique, which allows the addition of one nucleotide in a one-pot reaction of sequential coupling, oxidation and deprotection, followed by a single precipitation step. Furthermore, we demonstrate how to suppress depurination during the addition of adenine nucleotides. We showcase the potential of this technique to prepare high-purity 4-arm PEG-T_{20} (T = thymine) and 4-arm PEG-A_{20} building blocks in multi-gram scale. Such complementary 4-arm PEG-DNA building blocks reversibly self-assemble into supramolecular model network hydrogels, and facilitate the elucidation of bond lifetimes. These model network hydrogels exhibit new levels of mechanical properties, high stability at room temperature (melting at 44 °C), and thus open up pathways to next-generation, scalable DNA-materials programmable through sequence recognition and available for macroscale applications.

Introduction

DNA motifs present a powerful toolbox for mimicking the functional complexity of biological systems - such as recognition, programmable structure formation, information processing, communication, and replication.[1-7] Oligonucleotide sequences serve to program highly advanced structural features,[8-14] sensing and signaling mechanisms,[15-18] information processing,[19-22] and autonomous out-of-equilibrium systems.[23-27] The precise implementation of such functionalities is pivotal to designing the next generation of adaptive and interactive materials capable of autonomous and life-like behavior.[28] Indeed, current materials with DNA connecting motifs show increasingly advanced properties for applications as soft robotics,[29-30] therapeutic and cell culture hydrogels,[31-34] programmable fluorescent mechanosensing,[35] and materials responding to biological inputs.[36]

However, a lack of large-scale synthetic access to oligonucleotide building blocks currently prevents widespread application of DNA materials. Despite significant advances in biotechnological production and replication techniques,[37-38] the most widespread and versatile synthesis technique for DNA and RNA is solid-phase oligonucleotide synthesis (SPOS) based on phosphoramidite chemistry.[39-40] The 4-step nucleotide addition cycle – coupling, capping, oxidation, deprotection/detritylation – is performed on automated synthesizers using insoluble supports. The heterogeneous nature of this flow-chemistry method facilitates the fast and automated synthesis of sequences up to 200 nucleotides, but suffers from intrinsic scalability limitations and high reagent consumption. As an alternative strategy, liquid-phase oligonucleotide synthesis (LPOS) uses homogeneous reaction mixtures with, in principle, unlimited scalability, and requires significantly smaller reagent excesses.[41-42] In LPOS, oligonucleotides are grown from a soluble support, which can be separated from the reaction mixture after each step by precipitation,[43-48] extraction,[49] chromatography,[50] or nanofiltration.[51] The most prominent of these - the high efficiency liquid-phase (HELP) method - uses a polyethylene glycol (PEG) support, which is precipitated after each step. Although originally pioneered by Bonora *et al.* with the intention of cleaving the PEG-DNA conjugate after synthesis,[43-44] this technique has since been applied to the synthesis of PEG-DNA for materials applications. Tanaka *et al*. prepared 4-arm PEG-DNA building blocks with few nucleotides to form hydrogels via non-duplex interaction, such as G-quadruplex and C-based i-motifs.[52-53] Critically, these gelation principles only require short DNA sequences, and the presently available short length of a few nucleotides does indeed not allow for linking via DNA duplex hybridization in a suitable temperature

regime. Thus, they do not provide access to exploiting the programmable molecular recognition known from DNA. Indeed, the key limitation to accessing well-defined starPEG-DNA conjugates with long ssDNA sequences via liquid-phase on-PEG oligonucleotide synthesis is the laborious multistep reaction/purification nature involving 4-5 precipitation workups to complete one single nucleotide addition cycle, even if the capping step is skipped.[42, 52-53] Furthermore, the acidic detritylation step to deprotect the 5'-OH before the next nucleotide coupling is slow, partially reversible, and often not quantitative in the homogeneous liquid phase. This presents no problem in SPOS, where the cleaved 4,4'-dimethoxytrityl (DMT) protecting group is washed out continuously to shift the equilibrium, but, in LPOS, the extended acid exposure times cause significant backbone cleavage through depurination of adenine nucleotides (A).[41, 54] Hence, the synthesis of A-rich sequences presents another major bottleneck for LPOS.

Overcoming these limitations requires a drastic simplification of the liquid-phase on-PEG oligonucleotide synthesis and to rethink the chemistry involved. If applied to star-PEG, this synthesis would be the key to accessing high quality starPEG-DNA conjugate building blocks in large scale, that remain difficult to access using classical post-functionalization of star polymers with ssDNA sequences. Whereas the attachment of small molecules to DNA can be achieved using traditional post-conjugation techniques,[55-56] insufficient reactivity between end-functionalized DNA and reactive star-PEGs (or other polymers) makes starPEG-DNA conjugates difficult to obtain in high purity, definition, and large scale.[57-59] However, such well-defined star-DNA polymers would be interesting components for fundamental sciences and applications. For instance, star polymers with defined end-group connectivity facilitate the construction of model network materials, and are highly sought after for the topological design of network materials.[60-63] They enable the bottom-up design of macroscopic network properties based on molecular connecting motifs, which is important to fundamentally understand gelation, mechanical and topological behavior in networks, and enable precision hydrogel design for applications.[64-67]

In this work, we present the first synthesis strategy for a One-Pot – Liquid-Phase Oligonucleotide Synthesis (OP-LPOS), and use this method to prepare two different 4-arm PEG-DNA building blocks with 20 oligonucleotides per arm in 10-20 gram scale (**Scheme 1**). We merge the three steps required for one nucleotide addition cycle – coupling, oxidation, and detritylation – into a one-pot process with sequential reagent addition, requiring generally only a single precipitation to recover the product in high purity after the complete addition of the nucleotide. We focus on thymine and adenine

homo-repeats as those allow complementary interactions by duplex formation, and because adenine is the most challenging nucleobase with respect to depurination and chain cleavage.[54] Indeed, our detailed investigation of conditions, reagents, and substitution effects allows to suppress depurination and backbone cleavage for A-nucleotides and allows the clean liquid-phase synthesis of 4-arm PEG-A_{20}. We then combine these complementary building blocks (4-arm PEG-T_{20} and 4-arm PEG-A_{20}) to study the hybridized T_{20}-A_{20} duplexes as a mechanical connection in self-standing model network hydrogels with excellent mechanical strength.

Results and discussion

One-pot oligonucleotide addition

The primary bottleneck in liquid-phase oligonucleotide synthesis (LOPS) is the incompatibility of the reagents in each step, and the need for repeated precipitation and filtration after the coupling, oxidation, and detritylation steps, which is labor-intensive and causes product losses. Especially the coupling and detritylation steps are cumbersome, as they require repeated precipitations in diethyl ether to remove excess phosphoramidite reagent after coupling, and two detritylation steps are needed to drive the partially reversible deprotection to completion. The capping step is often omitted in LPOS due to the high coupling efficiencies achieved compared to heterogeneous SPOS, and in order to simplify the procedure.[51-53, 68]

Merging all three steps - coupling, oxidation, deprotection/detritylation - into a one-pot process with a single precipitation workup is the key to making large-scale PEG-DNA building block production feasible. The realization of this one-pot procedure requires to solve the following steps:

(1) Realizing an oxidation of the phosphite triester (P^{III}) without inducing the formation of side products or defects, immediately after coupling and without removal of the excess phosphoramidite reagent and tetrazole-based activator.

(2) Driving the partially reversible detritylation to completion in the presence of all reagents added during the coupling and oxidation steps.

(3) Isolation of the PEG-DNA conjugate in high yield and removing all reagents added during the entire one-pot process in ideally a single precipitation step at the very end of one cycle.

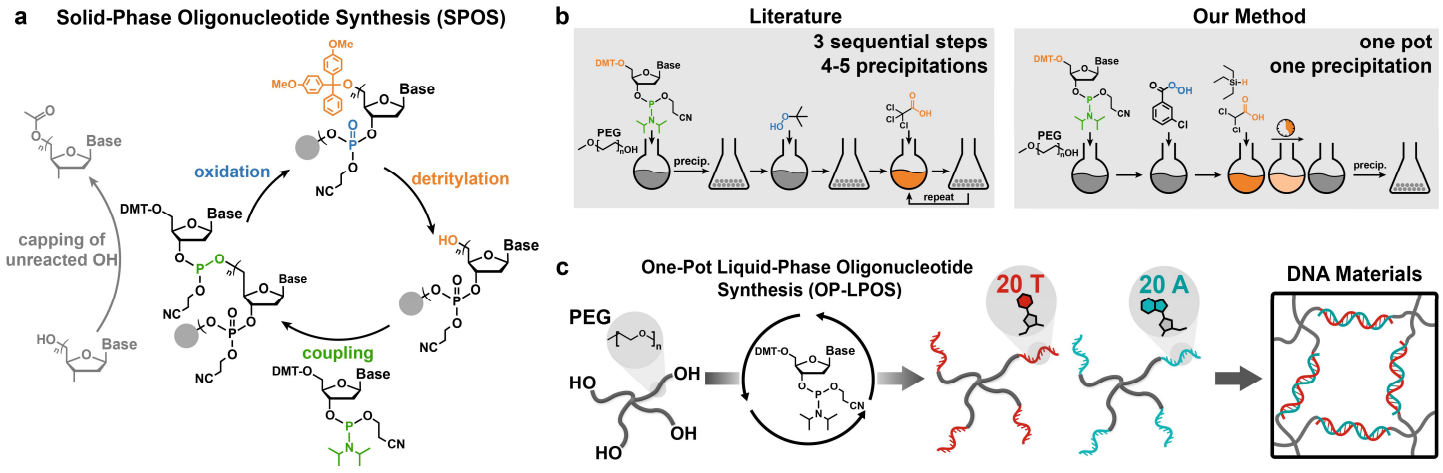

Scheme 1. Concept for One-Pot Liquid-Phase Oligonucleotide Synthesis (OP-LPOS) onto 4-arm PEG. (a) The four steps of the oligonucleotide synthesis cycle in SPOS. Note that capping is omitted in LPOS due to high coupling efficiency. **(b)** Overview of the reaction steps for DNA synthesis by classical LPOS following literature procedure and our OP-LPOS discussed in this work. **(c)** Schematic representation of the addition of 20 T and A nucleotides per arm onto 4-arm starPEG by OP-LPOS, followed by the self-assembly of ideal DNA network materials.

We establish this entire procedure by comparing each step of our developed one-pot procedure to state-of-the art conditions from two LPOS synthesis procedures in literature (**Scheme 1b**).[44, 53] We use commercially available narrowly dispersed 4-arm PEG-OH ($M_{n,\,MALDI}$ = 41,170 g/mol, $Đ$ = 1.04) as the starting material. Both solubility and precipitation benefit from a high molecular weight PEG support, especially for longer oligonucleotide sequences (>10 bases). In the coupling step, 4-arm PEG-OH is mixed with DMT-dT phosphoramidite and the activator 5-(ethylthio)-1*H*-tetrazole (ETT) in anhydrous acetonitrile. The excess of phosphoramidite to OH-groups varies in literature, with a 3-fold excess yielding 99-100% coupling efficiency.[69] Indeed, coupling 4-arm PEG-OH at 140 mg/mL in dry acetonitrile with 3 equivalents DMT-dT phosphoramidite and 12 equivalents (to OH groups) ETT activator yielded the 4-arm PEG-dT-DMT phosphite triester (P^{III}) with 100% coupling efficiency (determined by comparing the PEG signal to the T-methyl 3H in ^{1}H-NMR, **Figure S1-3**). The coupling step is identical to literature procedures in our work, except for the lack of workup by precipitation into diethyl ether after the coupling step.

Our key improvement over the established methods to directly continue in a one-pot process after the coupling is the replacement of the commonly used oxidation agent, *tert*-butyl hydroperoxide (TBHP), which is reported in literature to oxidize the isolated coupling product followed by another precipitation step (**Figure 1a-c, Figure S4**). Indeed, we first attempted to proceed with classical TBHP in a one-pot coupling and oxidation by adding the TBHP directly to the reaction mixture after the coupling step, without removing excess phosphoramidite or ETT. The use of a common 50-fold excess of TBHP (to the phosphoramidite) however led to the formation of a side product (**Figure 1d-f** top). A different procedure which uses a 10-fold excess of aqueous TBHP yielded similar results (**Figure S5-6**). An additional peak at 1.4-1.5 ppm in ^{1}H-NMR, and at -6 ppm in ^{31}P-NMR indicates the partial, unwanted substitution of the phosphite triester by TBHP or *t*-BuOH (which forms as a side product of oxidation with TBHP). Note that a control experiment, mixing of PEG-dT-DMT (P^{III}) with *t*-BuOH directly after coupling, did not result in this side product, indicating that its observation arises from a combination of the reactive TBHP with the reagents left over from the coupling step (**Figure S7**). In contrast, an oxidation of the phosphite triester in a one-pot fashion using *m*-chloroperoxybenzoic acid (mCPBA) resulted in a high-quality product without side reactions (**Figure 1e-f** bottom, **Figure S8-9**). Compared to TBHP, mCPBA has the important advantage that it reacts to *m*-chlorobenzoic acid upon oxidation, which is significantly less nucleophilic than *t*-BuOH.

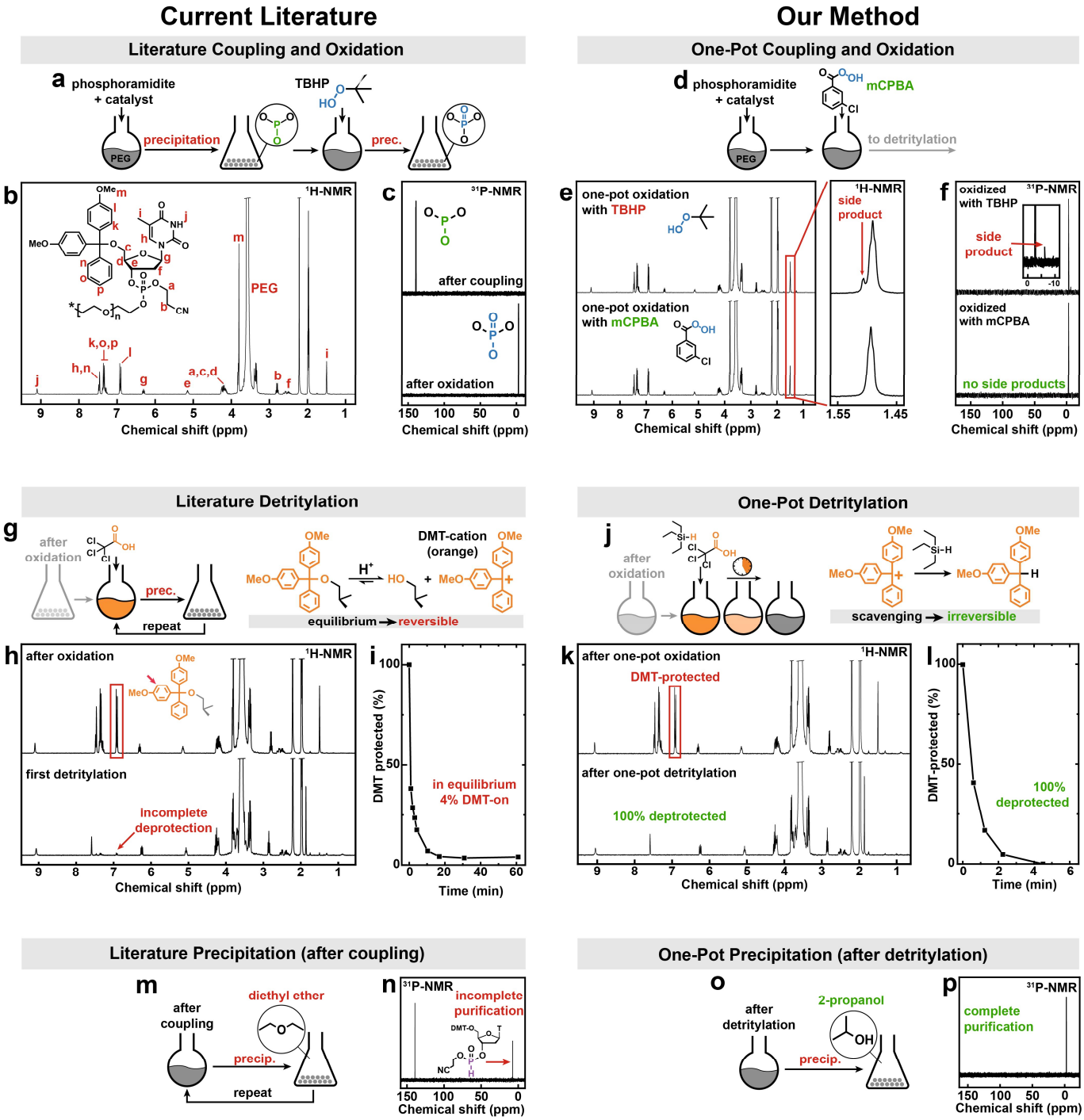

Figure 1. Comparison of the liquid-phase on-PEG oligonucleotide synthesis following current literature procedures (left) compared to our one-pot nucleotide addition process (right). (a) In literature, coupling and oxidation proceed with at least one precipitation after each step. **(b)** ^{1}H-NMR (CD_3CN) for 4-arm PEG-dT-DMT (P^{V}) isolated following literature procedure. **(c)** ^{31}P-NMR (CD_3CN) for 4-arm PEG-dT-DMT before and after oxidation, showing the phosphite triester (P^{III}) at 139 ppm and the phosphate triester (P^{V}) at -3 ppm. **(d)** One-pot coupling and oxidation by sequential addition of reagents without intermediate purification. **(e)** ^{1}H-NMR (CD_3CN) and **(f)** corresponding ^{31}P-NMR for the one-pot oxidation of 4-arm PEG-dT-DMT (P^{III}) by addition of the oxidizing agent directly to the reaction mixture after coupling. Top: TBHP 50 eq. at 0 ºC, bottom: mCPBA 2.5 eq. at room temperature to phosphoramidite. A side product forms for TBHP (red arrows in ^{1}H- and ^{31}P-NMR), but not for mCPBA. **(g)** Literature detritylation procedure requires repeated precipitation and reactions as detritylation is partially reversible. **(h)** ^{1}H-NMR (CD_3CN) for the removal of the DMT protecting group of 4-arm PEG-dT-DMT (P^{V}) in TCA/DCM following literature procedure. Top: before detritylation, bottom: after one detritylation step. **(i)** Reaction kinetics for the DMT-removal following literature conditions, resulting in an equilibrium of ca. 4% DMT-on during the first deprotection. **(j)** Our one-pot detritylation directly after oxidation is pushed to completion by the co-addition of a DMT-cation scavenger (TES). **(k)** ^{1}H-NMR (CD_3CN) before and after one-pot detritylation with TCA and TES in DCM directly after oxidation with mCPBA without intermediate purification, and **(l)** reaction kinetics plot showing complete detritylation in a single step. **(m)**

Removal of residual phosphoramidite reagent takes place after coupling in the literature procedure by repeated precipitation in diethyl ether. **(n)** ^{31}P-NMR (CD_3CN) of 4-arm PEG-dT-DMT (P^{III}) precipitated in diethyl ether once after coupling, showing residual H-phosphonate. **(o)** Removal of reagents in our one-pot procedure by a single precipitation into cold 2-propanol. **(p)** ^{31}P-NMR (CD_3CN) of PEG-dT-OH (P^V) precipitated into cold 2-propanol after a complete one-pot nucleotide addition cycle, showing only a single peak corresponding to the phosphate triester without any impurities. * Indicates the core of the 4-arm starPEG.

The last reaction step is the removal of the DMT protecting group (detritylation). This is a challenge, because it is an equilibrium reaction, commonly leading to incomplete detritylation in LPOS (**Figure 1g**). We first discuss the DMT deprotection of 4-arm PEG-dT-DMT (P^V) following literature conditions: the DMT-protected starting material (PEG-dT-DMT (P^V) previously isolated after oxidation by precipitation into diethyl ether) was dissolved (50 mg/mL) in dichloromethane (DCM) containing 30 mg/mL trichloroacetic acid (TCA) for deprotection. Indeed, after reaction and precipitation into diethyl ether, the ^{1}H-NMR shows incomplete deprotection with an equilibrium amount of 4% remaining DMT (**Figure 1h-i**). This partially deprotected product required re-dissolution in TCA/DCM solution and another precipitation into diethyl ether to achieve complete deprotection.

Achieving complete DMT removal in a one-pot process after coupling and oxidation and with full conversion requires to scavenge the released DMT-cation – orthogonal to all other reagents added and accumulated from the reactions before – to shift the equilibrium *in situ*. To achieve this, we added triethyl silane (TES) to the TCA/DCM reaction mixture after the oxidation step (which was conducted in a one-pot fashion after coupling). TES is a known DMT-cation scavenger[70] and shifts the equilibrium of the DMT deprotection to completion (**Figure 1j**). Indeed, adding 25 equivalents TCA (as a 600 mg/mL solution in DCM) and 15 equivalents TES (to DMT) after one-pot coupling and oxidation yields fully DMT-deprotected 4-arm PEG-dT-OH (P^V) in a single pot process orthogonal to all reagents previously added (**Figure 1k-l**). The scavenging of the DMT-cation – which has an intense orange color – results in a gradual discoloration of the reaction mixture, giving visual feedback for complete detritylation. In fact, ^{1}H-NMR analysis of samples collected in time intervals (**Figure 1l**) confirms the complete removal of the DMT group (5 min) before the orange color fully disappeared (9 min). The 4-arm PEG-T product synthesized by our OP-LPOS is fully identical to that synthesized following previous multistep procedures (**Figure S9**). Hence, there is no compromise on purity and quality.

As a final step, an efficient isolation protocol for the PEG-DNA is needed to remove all reagents by precipitation. This is another crucial improvement reported herein. In literature procedures, reagents are removed by precipitation into diethyl ether after each step. Aside from the double precipitation required to complete the detritylation step, the removal of the excess phosphoramidite and ETT after the coupling step by precipitation into diethyl ether is inefficient, leaving significant amounts of DMT-dT H-phosphonate (which forms upon hydrolysis of activated phosphoramidite) in the precipitate (**Figure 1m-n**). In fact, a full removal of all reagents from 4-arm PEG-dT-DMT (P^{III}) requires typically two additional re-precipitations from a solution in DCM (100 mg/mL polymer) into diethyl ether (**Figure S10).** After a screening of suitable solvents, we identified that the final reaction mixture, after the one-pot coupling, oxidation, and detritylation, can be completely purified by precipitation into 2-propanol at -30 ºC followed by washing with room temperature 2-propanol.

As a summary, the procedure optimized along these lines allows to obtain 4-arm PEG-dT-OH with excellent coupling efficiency (99%), highest purity, and high recovery yields (98.8%) (**Figure 1o-p**, ^{1}H-NMR in **Figure S8**). The procedure greatly reduces the time and solvent amounts needed to complete a nucleotide addition, and opens pathways for the synthesis of 4-arm PEG-DNA building blocks with long sequences for duplex hybridization in reasonable timescales – as we will show next.

Multi-gram synthesis of 4-arm PEG-T_{20}

After establishing the OP-LPOS technique for the addition of a first T-nucleotide onto the 4-arm PEG-OH, we used this technique to prepare high-quality building blocks for programmable DNA materials with a target 20-nucleotide sequence. The target product is a 4-arm PEG-T_{20}, using only T nucleotides to (1) facilitate characterization throughout the synthesis by ^{1}H-NMR spectroscopy and (2) to construct DNA materials with the complementary 4-arm PEG-A_{20} synthesized below. A focus on complementary 4-arm PEG-A_{20} will also allow us to demonstrate how to overcome depurination. Additionally, with an outlook on applications as hydrogels in mind, homo-repeats also make potential defects in one arm less critical for efficient hybridization compared to full sequence control.

To synthesize 4-arm PEG-T_{20}, we conducted the OP-LPOS onto 4-arm PEG-OH ($M_{n,\,MALDI}$ = 41,170 g/mol, $Đ$ = 1.04) 20 times (**Figure 2a**). Each coupling step was performed with a 3-fold excess of phosphoramidite and 12-fold excess of ETT to OH-groups for 60 minutes, added as 100 mM and 250 mM solutions in anhydrous acetonitrile respectively.

Following this, 2.5 equivalents (to phosphoramidite) of mCPBA were added as a powder, followed by stirring for 10 minutes. The 5'-DMT group was subsequently removed by adding 25 equivalents TCA (added as 600 mg/mL solution in DCM) and 15 equivalents TES to DMT groups. Discoloration again indicated complete detritylation in 10-15 minutes. One reaction cycle typically completes in 90 min. After the detritylation step, the reaction mixture was precipitated into -30 ºC 2-propanol, filtered, and the product washed with room temperature 2-propanol followed by diethyl ether. Whereas literature procedures report several co-evaporations with anhydrous acetonitrile to dry the material, we found that drying the product overnight on high vacuum (0.001 mbar) is sufficient prior to the next OP-LPOS.

To monitor the T_{20} growth, NMR spectra in DMSO-d_6 were measured of intermediate samples after each step (**Figure S11**), and the final ^{1}H-NMR spectrum shows the product free of impurities (**Figure 2c,** integration and ^{31}P-NMR in **Figure S12**). ^{31}P-NMR after each step readily verifies complete removal of the excess phosphoramidite reagent. The successful coupling was determined by comparing the thymine-3H integral to that of the 4-arm PEG-core in ^{1}H-NMR, and quantitative coupling is indicated in each step (**Table S1**). The amount of T compared to PEG is slightly higher than expected in the later synthesis steps, of which the origin is further discussed below. The initial 18.9 g scale synthesis yielded 9.0 g of 4-arm PEG-T_{20} (**Figure 2b**), and a total of 10.2 g of samples was collected throughout the synthesis (**Table S2**). The average recovery yield per step throughout the synthesis is 97.4%.

^{1}H-NMR spectra of the phosphate-protected product obtained after precipitation do not paint a complete picture as traces of unremoved phosphoramidite (after workup as the respective H-phosphonate) could in principal grow during each step into oligo-T chains not bound to PEG. To this end, we also performed an HPLC analysis of phosphate-deprotected samples (**Figure 2d**). HPLC reveals the desired PEG-DNA product with a clear shift of the growing PEG-T_n conjugate to earlier elution times due to increased hydrophilicity. Only a small amount of free oligo-T impurities is present, and the PEG-DNA purity can be quantified to 96% by mass after 20 steps (**Table S3**). Comparing the ratio of PEG-T_n over T_n oligos found by HPLC analysis to the ratio of T-to-PEG from ^{1}H-NMR integration gives further insights into the effective number of T nucleotides on the 4-arm PEG after each step (**Table S4**). This reveals a slight decrease in the coupling efficiency at later repetitions in the synthesis, which likely originates from reduced solubility and increased dilution for steps above 15 nucleotides. In order to remove oligo-T impurities and verify the actual number of T-nucleotides attached per arm, 4-arm PEG-T_{10}, -T_{15}, and T_{20} were purified by preparative HPLC and characterized

by ^{1}H-NMR spectroscopy (**Figure S13**). This reveals a coupling of 9.7 T, 13.8 T, and 17.7 T per arm for T_{10}, T_{15}, and T_{20} respectively. Agarose gel electrophoresis (AGE) further confirms successful growth of the PEG-DNA conjugate as evidenced by an increase of the band migration distance (**Figure 2e**). Although DNA samples generally migrate slower in AGE with increasing size, in this case the charge-to-mass ratio of the PEG-DNA conjugate increases during the synthesis, causing a faster band migration with increasing nucleotide count. This relative increase in migration distance becomes smaller as the PEG-DNA conjugates grow in T length, because the charge-to-mass ratio increases more slowly. SEC characterization similarly shows a narrow molecular weight distribution both with and without the cyanoethyl (CE) protecting group on the phosphate (**Figure S14**). The CE-group can be removed from the phosphate in concentrated ammonia/methylamine solution (AMA) for 30 minutes at room temperature after completion of the synthesis to the desired T_n length (**Figure S15**).

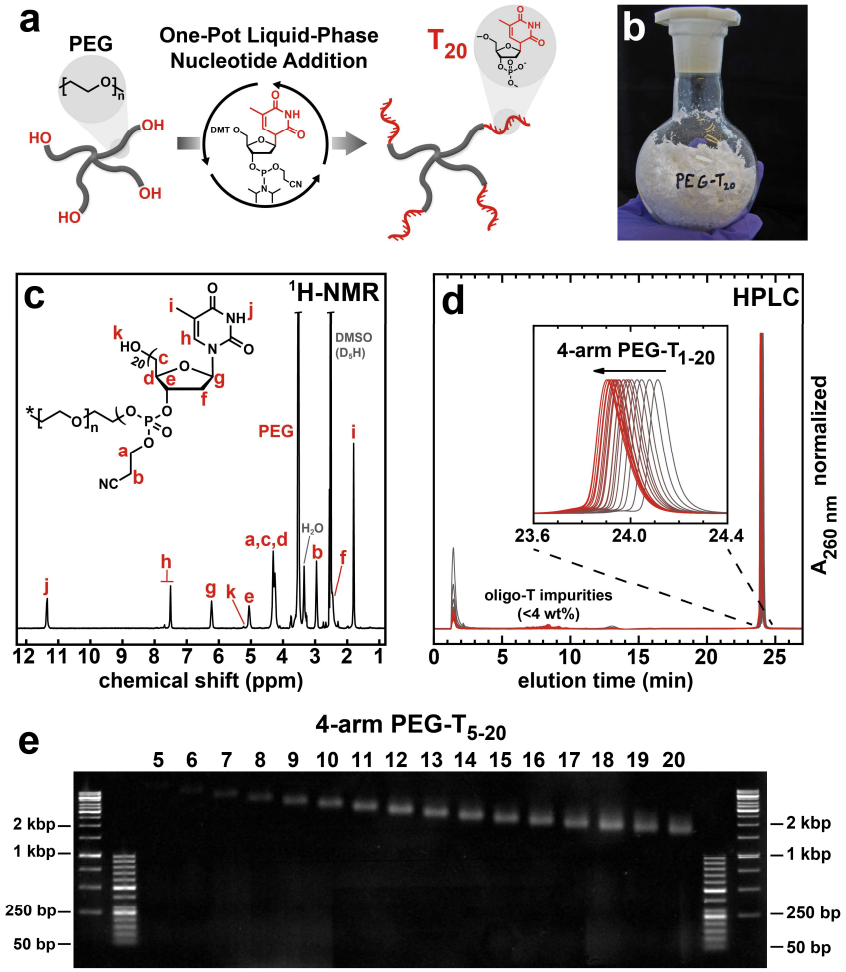

Figure 2. Synthesis of 4-arm PEG-T_{20} from 4-arm PEG-OH by OP-LPOS repeated 20 times. (a) General scheme. **(b)** Photograph of the 4-arm PEG-T_{20} product (phosphate protected). **(c)** ^{1}H-NMR (DMSO-d_6) of the product still bearing the CE protection group at the phosphate. **(d)** HPLC chromatogram of samples collected throughout the synthesis (phosphate was deprotected 30 minutes in AMA solution and diluted with

phosphate buffer). An inset shows the increasing hydrophilicity by shift of the elution time as the DNA content increases. **(e)** Agarose gel electrophoresis (AGE) of the phosphate-deprotected samples collected throughout the synthesis showing a faster band migration due to the increasing charge-to-mass ratio of the PEG-DNA conjugate (1.5 wt% agarose in tris-acetate EDTA buffer, 80 V constant, 60 min using in-cast staining with Roti-GelStain).

The main bottleneck throughout the synthesis is the increasingly poor solubility of the growing 4-arm PEG-DNA conjugate in acetonitrile and DCM, despite the high molecular weight of the PEG support. This leads to slower dissolution and higher viscosity at the beginning of the coupling step, as well as difficulties with precipitation and drying due to the fiber-like properties of the precipitate after 7-8 nucleotides are attached. To mitigate these problems, we recommend adding additional anhydrous acetonitrile during the coupling step, and additional DCM prior to precipitation (increasing the volume of 2-propanol proportionally) as the oligonucleotide sequence grows. The temperature of the 2-propanol for precipitation was increased from initially -30 ºC after the first nucleotide to room temperature after 9 nucleotides. From 11 nucleotides onwards, an additional re-precipitation from acetonitrile/DMSO (95/5 vol/vol) into diethyl ether was performed to facilitate efficient drying, as the product precipitated as dense fiber aggregates in 2-propanol which would be difficult to dry efficiently under vacuum in a single night.

Suppression of the depurination in A synthesis

Constructing DNA materials with a focus on model networks formed by two interacting 4-arm-PEG-DNA star polymers requires the synthesis of complementary 4-arm PEG-A_{20}. In fact, sequences with significant amounts of adenine nucleotides (in this case 80 per 4-arm PEG) are still a major bottleneck in LPOS, because long acid exposure times required for the acid-catalyzed detritylation induce depurination (removal of the adenine or guanine nucleobase; both are purine nucleobases).[41] This in turn leads to chain scission upon workup (**Figure 3a**). Adenine is considered more challenging compared to guanosine with respect to depurination,[54] which is why we focus on implementing the one-pot procedure for the 4-arm PEG-A_n synthesis. Particularly the most common A-nucleotide phosphoramidite (which has a benzoyl protecting group) is susceptible to depurination. This is of no concern in SPOS, as the continuous washing out of cleaved DMT groups speeds up the partially reversible deprotection (**Figure 3b**) and minimizes acid exposure. In order to solve this problem and facilitate the synthesis 4-arm PEG-A_{20}, we first discuss the optimization of our OP-LPOS to prevent depurination for benzoyl-protected A.

Understanding the nature of the problem is important: Indeed, not the speed of the depurination side reaction alone is important, but primarily the relative reaction rates of detritylation (DMT-removal) vs. depurination (adenine loss) are. To optimize the OP-LPOS and minimize depurination, we therefore determined both the detritylation and depurination reaction rates for various conditions during the one-pot addition of benzoyl-protected A-phosphoramidite to 4-arm PEG-OH. The degree of detritylation and depurination were monitored by collecting samples in time intervals and measuring ^{1}H-NMR to determine the remaining amounts of DMT (4H) and adenine (2H) at the PEG end group to the PEG arm (**Figure 3c-d,** highlighted by colored arrows). Both reactions follow first-order kinetics with good accuracy (**Figure 3e**). Therefore, we can define the "efficiency" of the detritylation step in our one-pot procedure as the ratio of the time constants of the depurination (τ_{dep}) over the detritylation (τ_{det}) reaction, which are the inverse slopes of the respective first order kinetic plots. A high efficiency value therefore means that the depurination reaction is slow relative to the detritylation reaction. The actual rate of detritylation is of lesser concern, provided detritylation proceeds in a comparably reasonable timeframe (2 min < τ_{det} < 20 min).

We started the optimization of the detritylation step (conducted in a one-pot fashion following coupling and oxidation of Bz-protected A, **Figure S16**) by probing the most influential parameters for the deprotection: (1) the type of acid and (2) the reaction temperature. Both trichloroacetic acid (TCA) and dichloroacetic acid (DCA) are used in oligonucleotide synthesis, with the former being stronger and achieving faster detritylation at lower concentrations. TCA was added in 30 eq. to DMT groups, and DCA in 60 eq. to DMT groups (both 600 mg/mL solutions in DCM; added directly after coupling with 3 eq. phosphoramidite and 12 eq. ETT to OH-groups, and one-pot oxidation with 2.5 eq. mCPBA to phosphoramidite). The DMT-cation scavenger TES was added as a 25-fold excess to DMT groups in all experiments. Although the acid concentration influences the detritylation rate more than the TES concentration, a larger excess of TES is desirable as this increases the detritylation rate somewhat without affecting depurination.

Detritylation experiments with both TCA and DCA show a strong increase in efficiency at 0 ºC compared to room temperature (**Figure 3f,** full kinetics in **Figure S17**). This corresponds to a preferred shift of better deprotection over suppressed depurination. Although 30 eq. TCA is more efficient than 60 eq. DCA at room temperature, the efficiency gain for DCA is higher during cooling, with the detritylation reaction being 5000 times faster than unwanted depurination at 0 ºC. Although the cooling slows down the detritylation reaction (as expected), the overall reaction time

stays within a reasonable range (τ_{det} = 17 min) and the reaction mixture is colorless after 171 min. We then investigated the effect of the molar excess of the preferred DCA to the coupled and oxidized DMT-protected nucleotide at 0 ºC. An increase of the excess of the acid increases the efficiency (**Figure 3g**, full kinetics in **Figure S18**). Hence, interestingly, cooling aids the efficiency, and adding more acid also aids the efficiency at 0 ºC. The reason for this is that the influence of a higher acid concentration decreases τ_{det} more than it increases τ_{dep}. This adds a convenience aspect in running the reactions, by requiring shorter detritylation times (time until reaction mixture is colorless: 295 min with 50 eq., 171 min with 60 eq., and 109 min with 70 eq. DCA at 0 ºC). Thus, the best reaction conditions are detritylation at 0 ºC with a large excess of DCA relative to DMT groups.

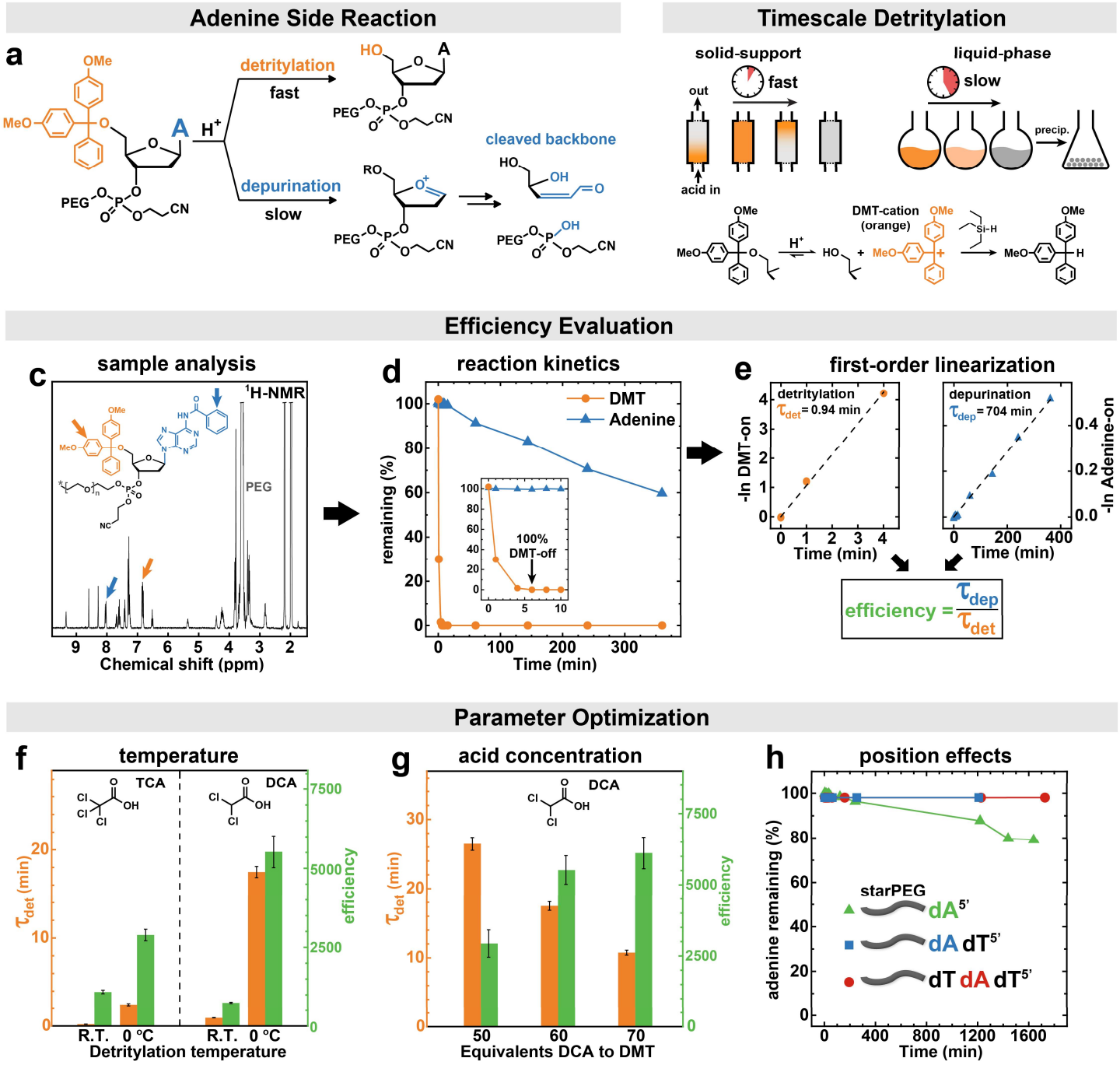

Figure 3. Suppression of depurination side reactions for adenine nucleotides. (a) Reaction scheme showing the acid-induced detritylation (DMT removal) and depurination reaction, which leads to loss of purine nucleobases (A and G) followed by chain scission after workup. **(b)** Scheme showing how the heterogeneous nature of SPOS leads to faster detritylation and thus less depurination than in OP-LPOS. **(c)** ^{1}H-NMR (CD_3CN) of 4-arm PEG-A-OH after coupling and oxidation, showing the two peaks that are integrated and compared to the PEG-arm for monitoring the degree of detritylation (orange, DMT-4H) and depurination (blue, benzyl protecting group 2H). **(d)** Example of a single detritylation/depurination experiment kinetic plot showing the amount of DMT and adenine remaining per PEG-arm vs. time. **(e)** Linearization of the detritylation and depurination reaction rates assuming first-order kinetics, which gives the inverse of the time constant as the slope. The efficiency of the detritylation is defined as the time constant of the depurination divided by that of the detritylation reaction. **(f)** Efficiency and detritylation time constant for TCA (30 eq. to DMT) and DCA (60 eq. to DMT) at two different temperatures and **(g)** for various equivalents of DCA to DMT at 0 °C. **(h)** Depurination vs. time for an A-nucleotide at three different positions (PEG-A, PEG-A-T, and PEG-T-A-T) with TCA 30 eq. to DMT at 0 °C.

Although depurination is 6100 times slower than detritylation under our best conditions (70 eq. DCA at 0 ºC), this value may still be problematic for the synthesis of 4-arm PEG-A_{20}, simply because innerlying A_n-segments are repeatedly exposed to acid, and depurination of these would induce chain scission leading to the loss of an entire oligonucleotide arm. Fortunately, it was suggested that 5'-terminal A-nucleotides are significantly more susceptible to depurination than A nucleotides incorporated in a growing chain (end group effect).[54, 71] To investigate this end group effect for our procedure, we tested this using 30 eq. TCA at 0 ºC for model end group structures, by adding a T unit after an A unit, or by flanking A by one T before and after it. T was chosen to avoid overlapping signals in NMR analysis. We chose the more aggressive TCA here rather than the more efficient DCA because the depurination timescales are easier to observe. Indeed, whereas 4-arm PEG-A shows 20% depurination after 24 hours (reaction mixture is colorless in 22 min, indicating all DMT scavenged), both 4-arm PEG-A-T and PEG-T-A-T show no measurable depurination at all over the course of 24 hours after addition of TCA. (**Figure 3h**). This confirms that A-nucleotides inside a growing oligonucleotide structure are indeed protected against depurination.

Taken together, our quantitative approach to understand the involved reactions now enables efficient detritylation that (1) induces negligible depurination for the 5'-terminal A-nucleotide, and (2) shows no measurable depurination at all for internal A-nucleotides. We will exploit this development in the next step for the synthesis of 4-arm PEG-A_{20} which is complementary to the synthesized 4-arm PEG-T_{20}.

Multi-gram synthesis of 4-arm PEG-A_{20}

The synthesis of 4-arm PEG-A_{20} proceeds in a similar fashion to the 4-arm PEG-T_{20}, but with the main difference being the detritylation conditions. We started with the same 4-arm PEG-OH ($M_{n,\,MALDI}$ = 41,170 g/mol, $Đ$ = 1.04) and repeated the OP-LPOS with Bz-protected A-phosphoramidite 20 times (**Figure 4a**). We again used a 3-fold excess of phosphoramidite and a 12-fold excess of ETT relative to OH-groups in the coupling step, followed by addition of 2.5 eq. mCPBA (to phosphoramidite) for oxidation, which takes 10 minutes. After cooling down to 0 ºC, detritylation was triggered by adding DCA (70 eq. to DMT groups) as a 600 mg/mL solution in DCM, and neat TES (25 eq. to DMT). The reaction mixture becomes orange upon addition of the acid, and detritylation was over when the mixture almost loses its orange color (generally around 100 minutes at 0 ºC). The reaction mixture was precipitated into -30 ºC 2-propanol, filtered, and washed with 2-propanol. Due to the significantly larger size of the benzoyl-protected A-

nucleotide, a second precipitation from DCM (in the last 5 steps from DMSO) into 2-propanol was required to completely remove all impurities. Each product was washed with diethyl ether after filtration, and dried overnight on high vacuum.

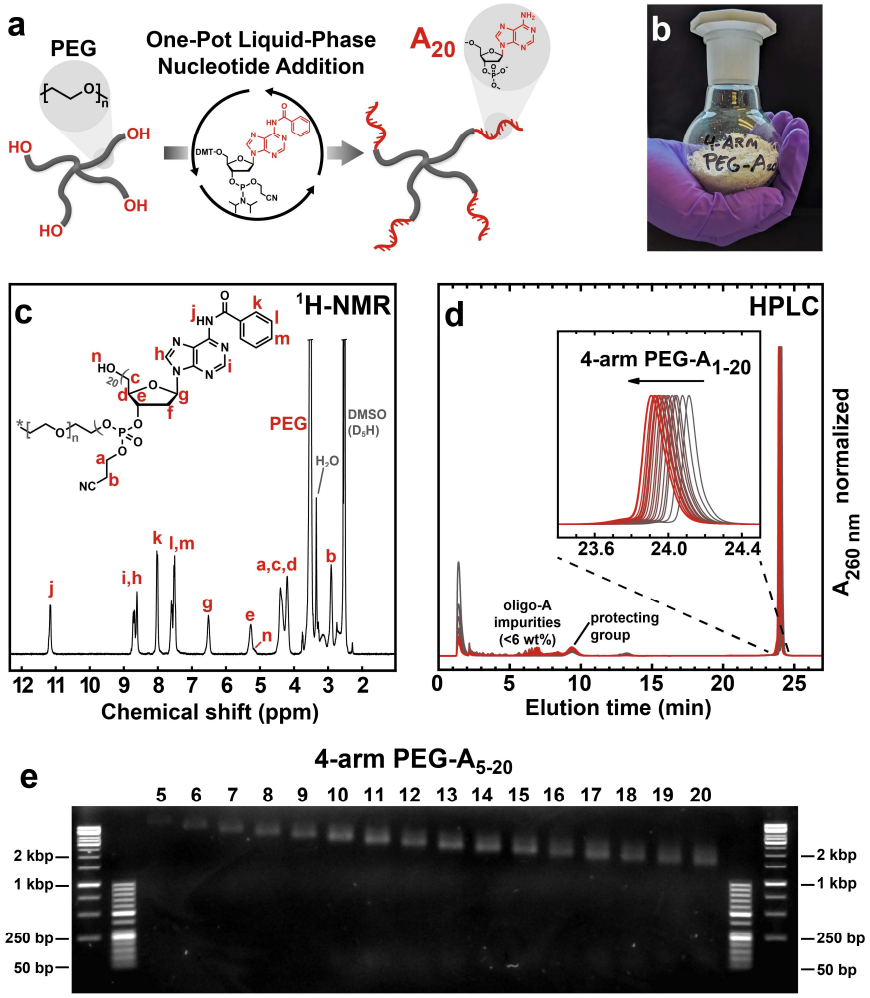

Figure 4. Synthesis of 4-arm PEG-A$_{20}$ from 4-arm PEG-OH by OP-LPOS repeated 20 times. (a) General scheme. **(b)** Photograph of the 4-arm PEG-A$_{20}$ product (with both Bz- and CE-protecting groups). **(c)** ^{1}H-NMR (DMSO-d$_6$) of the product still bearing the CE protection group at the phosphate and benzoyl protecting group on the adenine nucleobase. **(d)** HPLC chromatogram of samples collected throughout the synthesis (deprotected 120 minutes in AMA solution and diluted with phosphate buffer). An inset shows the increasing hydrophilicity as the DNA content increases. **(e)** Agarose gel electrophoresis (AGE) of the deprotected samples collected throughout the synthesis, depicting a faster band migration because of the increasing charge-to-mass ratio (1.5 wt% agarose in tris-acetate EDTA buffer, 80V constant, 60 min using in-cast staining with Roti-GelStain).

10.1 gram of 4-arm PEG-OH after 20 one-pot nucleotide addition steps yielded 3.9 gram of 4-arm PEG-A$_{20}$ with the Bz- and CE-groups on the adenine and phosphate respectively (**Figure 4b**), and an additional 4.1 gram of samples was collected throughout the synthesis (**Table S5**). The average recovery yield per step throughout the synthesis is 95.2%.

After each step, ^{1}H-NMR and ^{31}P-NMR spectra in DMSO-d_6 verify successful coupling and purification (**Figure S19**). **Figure 4c** shows the ^{1}H-NMR spectrum of the final product (adenine- and phosphate-protected) without impurities (integrated spectrum and ^{31}P-NMR in **Figure S20**). Integration of ^{1}H-NMR spectra again shows the expected amounts of adenine units relative to the 4-arm PEG-core in each step (**Table S6**). Similar to above, HPLC chromatograms of 4-arm PEG-$A_{1\text{-}20}$ (deprotected 2 hours in AMA solution, then diluted with phosphate buffer) depict a small amount of oligo-A impurities appearing throughout the synthesis (**Figure 4d**). Similar to the synthesis of 4-arm PEG-T_{20}, the amount of oligo-A impurities is small until 15 nucleotides and increases in the last steps. Nonetheless, HPLC measurements show that the final 4-arm PEG-A_{20} makes up 94 wt%, while only 6 wt% oligo-A contaminants are present (**Table S7**). A comparison of the molar purity of PEG-A_n (relative to oligo-A impurities) from HPLC measurements with the A-to-PEG ratio from ^{1}H-NMR integration reveals a slight decrease in coupling efficiency towards the end of synthesis similar to the 4-arm PEG-T_{20} synthesis (details **Table S8**). This again arises from decreased solubility and increased dilution as the synthesis proceeds. We purified 4-arm PEG-A_{10}, -A_{15}, and -A_{20} by preparative HPLC to isolate the product free of any oligo-A impurities, and measured ^{1}H-NMR to determine the actual number of A-nucleotides attached per PEG-arm (**Figure S21**). Integration of the adenine protons in ^{1}H-NMR relative to the PEG-arm gives an actual coupling of 9.2 A, 13.1 A, and 17.2 A per arm for targeted 4-arm PEG-A_{10}, -A_{15}, -A_{20}. Importantly, the number of A relative to PEG is similar to that observed in the 4-arm PEG-T_{20} preparation throughout the synthesis, which indicates that indeed depurination is efficiently prevented. Gel electrophoresis of deprotected samples for 4-arm PEG-$A_{5\text{-}20}$ also confirms the excellent quality of the material (**Figure 4e**). Each step shows a steady increase in the band migration distance, indicating efficient coupling and no disintegration of the product as the synthesis proceeds (which would result in chain scission, especially for the innermost nucleotides). In the interest of a complete discussion, SEC analysis did not lead to meaningful results for the Bz- and phosphate-protected 4-arm PEG-A_{20} due to interactions with the SEC columns, and deprotected 4-arm PEG-A_{20} is not soluble in the SEC solvent (DMAc with 0.5 % LiBr).

In summary, the analysis methods discussed describe a well-defined 4-arm PEG-A_{20} building block of good quality, with only limited oligo-A impurities and no visible depurination or chain scission. We stress the importance of this achievement, as depurination has until now been a major bottleneck in LPOS.[41] The synthesis of 4-arm PEG-A_{20} by our OP-LPOS shows that this technique is not only a major step forward in synthesis times and accessible DNA length, but

the new deprotection strategy expands the scope of accessible oligonucleotide sequences for LPOS in general to sensitive adenine.

4-arm PEG-DNA model networks

With access to both 4-arm PEG-T_{20} and 4-arm PEG-A_{20} in good quality and large scale, we demonstrate the application of such building blocks in supramolecular model network hydrogels crosslinked by DNA duplex hybridization of complementary building blocks (**Figure 5a**). Supramolecular networks constructed from A-B functional 4-arm building blocks offer unique insights into bond dynamics owing to the defined network topology.[62] Hydrogels constructed from complementary DNA sequences additionally allow melting and cooling of the network to ensure an ideal topology by annealing of defects.

The duplex melting temperature of an A_{20}/T_{20} sequence can be calculated using oligo analyzer tools to 58 °C at 150 mM Na^+ and 3.6 mM DNA (55 °C for A_{17}/T_{18}), hence sufficiently above room temperature. To ensure an ideal network topology, we first determined the overlap concentration of the 4-arm PEG-OH by rheology, and found it to be at 3.7 wt% or 0.90 mM in water (**Figure S22**). The PEG-DNA hydrogel was thus constructed by mixing equal volumes of 4-arm PEG-A_{20} and –T_{20} both at 0.90 mM in phosphate buffer (150 mM Na^+) at 60 °C , followed by slow cooling to room temperature to anneal the structure.

The high stability of the long A-T duplex manifests itself as high shape-stability at room temperature. The hydrogel (pieces of several cm^3) can be molten and poured into various shapes without any visible flow at room temperature (**Figure 5b**). Oscillatory rheological analysis gives more quantitative insights into the dynamics of the A-T duplex crosslinks in the hydrogel. Temperature sweeps in the rheometer at f = 1 Hz show a crossover of the storage modulus G' and loss modulus G'' at 44 ºC (**Figure 5c**), which corresponds to the gel-to-sol transition. This compares reasonably well to the calculated T_m of 55 ºC of an individual duplex as the gel-to-sol transition does not require the melting of all duplexes. This clearly shows the success in constructing macroscale model network DNA-crosslinked materials from sufficiently long oligonucleotide sequences. Due to the model network topology, the dynamics of the A-T duplex can be further elucidated by a rheological frequency sweep, which reveals the visco-elastic behavior of the material over different timescales. Indeed, a frequency sweep at 25 ºC shows the high stability of the duplex up to very long timescales (**Figure 5d**). The crossover of the storage and loss moduli at 0.00125 Hz, which correlates to a relaxation time of 800

s or 13.3 min., is indicative of the bond exchange timescale. This relaxation time scale corresponds to significantly enhanced stability than for comparable multi-arm DNA hydrogel systems, which generally show relaxation times in the range of 0.1 to 10 seconds.[26, 72-74] This may be the the result of the PEG-DNA network nature, which provides more flexibility compared to the stiff all-DNA networks. From a material perspective, it is important to emphasize that these gels have storage moduli G' > 1000 Pa and form self-standing, shape-persistent gels with sizes of several cm^3 (**Figure 5b**), while most other DNA gels known to date have very limited shape stability under their own weight and feature G' values in the range of a few Pa to 100 Pa. The high stability of the hydrogel crosslinked by the A-T duplex underscores the importance of synthesizing long oligonucleotide sequences onto 4-arm PEG. We expect the important material characteristics, such as bond lifetime, G' values and T_m values, to be tunable by changing the concentration and by changing the duplex overlap length in order to suit diverse applications. We will address this in forthcoming publications. Additionally, large scales (see e.g. 50 mL centrifuge tube in **Figure 5b**) are now accessible to construct DNA materials with a temperature profile (gel-sol transition at 44 °C) applicable to room temperature studies as well as cell studies at 37 °C.

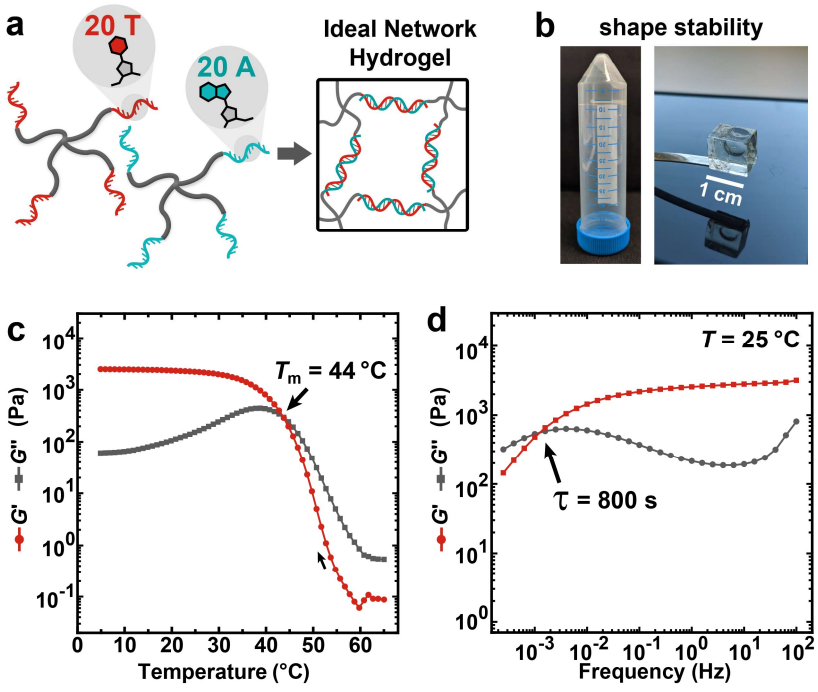

Figure 5. Formation of model network hydrogels from 4-arm PEG-T_{20} and –A_{20} building blocks. (a) Scheme. **(b)** Photographs showing the hydrogel (0.9 mM PEG-DNA total) which has high shape stability at room temperature. **(c)** Temperature sweep of the hydrogel upon cooling whilst measuring oscillatory rheology (f = 1 Hz, γ = 10%, 2 °C/min). **(d)** Oscillatory frequency sweep of the hydrogel at 25 °C (γ = 10%), showing the crossover of G' and G'', which reveals the bond relaxation time as the inverse of the crossover frequency.

Conclusions

We introduced the first one-pot liquid-phase DNA synthesis process for long ssDNA sequences tethered to polymers, which allows the addition of one nucleotide in a one-pot reaction (coupling, oxidization, detritylation) followed by a single precipitation step. The key to success is choosing the right oxidizing agent, the scavenging of the DMT-cations during detritylation, and precipitation in 2-propanol rather than diethyl ether. We further optimized reaction conditions to also enable for the first time the depurination-free addition of A-nucleotides with this process. Using a large excess of dichloroacetic acid rather than trichloroacetic acid in an ice bath suppresses depurination side reactions, and we further demonstrated that no depurination is visible at all for internal (5'-substituted) A-nucleotides. To demonstrate the feasibility of synthesizing 4-arm PEG building blocks with oligonucleotide chains long enough for DNA duplex hybridization, we synthesized 4-arm PEG-T_{20} and 4-arm PEG-A_{20} by 20-time repeated OP-LPOS in multigram scale. Hydrogels constructed from these building blocks form shape-persistant free standing large objects, and show high bond stability with a gel-to-sol transition of 44 ºC and extended bond lifetimes, thus delivering on the premise of synthesizing long oligonucleotide sequences. Such functional supramolecular model networks formed from complimentary star polymers can offer unique insights into bond dynamics and binding constants, and the synthetic procedure discussed in this work opens up pathways to more advanced studies on DNA as a mechanical crosslink. In terms of bottom-up biomaterials design, the high stability of the model network starPEG-DNA hydrogels in terms of T_m and bond lifetimes is crucial for cell culture and artifical tissue supports, which require the precise programming of properties, biomacromolecular functional groups, and cellular signalling capabilities at 37 ºC.

The reagents and solvents used in this work are largely standard, and we expect that this one-pot on-PEG technique will be compatible with other currently promising liquid-phase oligonucleotide synthesis processes such as nanofiltration, and with other types of supports. In order to achieve full sequence control in OP-LPOS and to synthesize sequences with guanine (G) and cytosine (C) in the future, the synthesis procedure must be validated for those and possibly adapted to achieve compatibility of a single set of reaction conditions with all nucleobases. We believe that the adenine (A) synthesis is however the most critical part among all nucleobases. Building on this, we expect that further investigations will successfully incorporate the sequences with G- and C-nucleotides, overcome solubility limitations, and expand to different types of macromolecular supports. The possibility of combining any desired synthetic polymer architecture

with fully programmable DNA sequences in large scale and excellent quality has the potential to sustainably expand DNA materials science in both scope and scale.

Conflicts of interest

The authors declare no conflicts of interest.

Acknowledgements

This work was supported by the European Research Council starting Grant (TimeProSAMat) Agreement 677960, and the Deutsche Forschungsgemeinschaft (DFG, German Research Foundation) under Germany's Excellence Strategy – EXC-2193/1 – 390951807 via "Living, Adaptive and Energy-Autonomous Materials Systems" (livMatS).

References

1. Kohman, R. E.; Kunjapur, A. M.; Hysolli, E.; Wang, Y.; Church, G. M., From Designing the Molecules of Life to Designing Life: Future Applications Derived from Advances in DNA Technologies. *Angew. Chem., Int. Ed.* **2018,** *57* (16), 4313-4328.
2. Heinen, L.; Walther, A., Celebrating Soft Matter's 10th Anniversary: Approaches to program the time domain of self-assemblies. *Soft Matter* **2015,** *11* (40), 7857-66.
3. Hu, Y.; Niemeyer, C. M., From DNA Nanotechnology to Material Systems Engineering. *Adv. Mater.* **2019,** *32* (26), 1806294.
4. Figg, C. A.; Winegar, P. H.; Hayes, O. G.; Mirkin, C. A., Controlling the DNA Hybridization Chain Reaction. *J. Am. Chem. Soc.* **2020,** *142* (19), 8596-8601.
5. Hendrikse, S. I. S.; Gras, S. L.; Ellis, A. V., Opportunities and Challenges in DNA-Hybrid Nanomaterials. *ACS Nano* **2019,** *13* (8), 8512-8516.
6. Seeman, N. C.; Sleiman, H. F., DNA nanotechnology. *Nat. Rev. Mater.* **2017,** *3* (1), 17068
7. Merindol, R.; Walther, A., Materials learning from life: concepts for active, adaptive and autonomous molecular systems. *Chem. Soc. Rev.* **2017,** *46* (18), 5588-5619.
8. Nummelin, S.; Kommeri, J.; Kostiainen, M. A.; Linko, V., Evolution of Structural DNA Nanotechnology. *Adv. Mater.* **2018,** *30* (24), 1703721.
9. Loescher, S.; Groeer, S.; Walther, A., 3D DNA Origami Nanoparticles: From Basic Design Principles to Emerging Applications in Soft Matter and (Bio‐) Nanosciences. *Angew. Chem., Int. Ed.* **2018,** *57* (33), 10436-10448.
10. Merindol, R.; Loescher, S.; Samanta, A.; Walther, A., Pathway-controlled formation of mesostructured all-DNA colloids and superstructures. *Nat. Nanotechnol.* **2018,** *13* (1), 730–738.
11. Zhang, F.; Nangreave, J.; Liu, Y.; Yan, H., Structural DNA nanotechnology: state of the art and future perspective. *J. Am. Chem. Soc.* **2014,** *136* (32), 11198-211.
12. McLaughlin, C. K.; Hamblin, G. D.; Hanni, K. D.; Conway, J. W.; Nayak, M. K.; Carneiro, K. M.; Bazzi, H. S.; Sleiman, H. F., Three-dimensional organization of block copolymers on "DNA-minimal" scaffolds. *J. Am. Chem. Soc.* **2012,** *134* (9), 4280-6.
13. Serpell, C. J.; Edwardson, T. G.; Chidchob, P.; Carneiro, K. M.; Sleiman, H. F., Precision polymers and 3D DNA nanostructures: emergent assemblies from new parameter space. *J. Am. Chem. Soc.* **2014,** *136* (44), 15767-15774.
14. Jones, M. R.; Seeman, N. C.; Mirkin, C. A., Programmable materials and the nature of the DNA bond. *Science* **2015,** *347* (6224), 1260901.
15. Del Grosso, E.; Amodio, A.; Ragazzon, G.; Prins, L. J.; Ricci, F., Dissipative Synthetic DNA-Based Receptors for the Transient Loading and Release of Molecular Cargo. *Angew. Chem., Int. Ed.* **2018,** *57* (33), 10489-10493.
16. Raddaoui, N.; Stazzoni, S.; Möckl, L.; Viverge, B.; Geiger, F.; Engelke, H.; Bräuchle, C.; Carell, T., Dendrimer‐Based Signal Amplification of Click‐Labelled DNA in Situ. *ChemBioChem* **2017,** *18* (17), 1716-1720.
17. Kwon, P. S.; Ren, S.; Kwon, S.-J.; Kizer, M. E.; Kuo, L.; Xie, M.; Zhu, D.; Zhou, F.; Zhang, F.; Kim, D.; Fraser, K.; Kramer, L. D.; Seeman, N. C.; Dordick, J. S.; Linhardt, R. J.; Chao, J.; Wang, X., Designer DNA architecture offers precise and multivalent spatial pattern-recognition for viral sensing and inhibition. *Nat. Chem.* **2019,** *12* (1).
18. Pandey, S.; Kankanamalage, D. V. W.; Zhou, X.; Hu, C.; Isaacs, L.; Jayawickramarajah, J.; Mao, H., Chaperone Assisted Host-Guest Interactions Revealed by Single-Molecule Force Spectroscopy. *J. Am. Chem. Soc.* **2019,** *141* (46), 18385-18389.
19. Woods, D.; Doty, D.; Myhrvold, C.; Hui, J.; Zhou, F.; Yin, P.; Winfree, E., Diverse and robust molecular algorithms using reprogrammable DNA self-assembly. *Nature* **2019,** *567* (7748), 366–372.
20. Thubagere, A. J.; Li, W.; Johnson, R. F.; Chen, Z.; Doroudi, S.; Lee, Y. L.; Izatt, G.; Wittman, S.; Srinivas, N.; Woods, D.; Winfree, E.; Qian, L., A cargo-sorting DNA robot. *Science* **2017,** *357* (6356).
21. Su, H.; Xu, J.; Wang, Q.; Wang, F.; Zhou, X., High-efficiency and integrable DNA arithmetic and logic system based on strand displacement synthesis. *Nat. Commun.* **2019,** *10* (1), 5390.
22. O'Reilly, R. K.; Turberfield, A. J.; Wilks, T. R., The evolution of DNA-templated synthesis as a tool for materials discovery. *Acc. Chem. Res.* **2017,** *50* (10), 2496-2509.

23. Deng, J.; Walther, A., Pathway Complexity in Fuel-Driven DNA Nanostructures with Autonomous Reconfiguration of Multiple Dynamic Steady States. *J. Am. Chem. Soc.* **2019,** *142* (2), 685-689.
24. Heinen, L.; Walther, A., Programmable dynamic steady states in ATP-driven nonequilibrium DNA systems. *Sci. Adv.* **2019,** *5* (7), eaaw0590.
25. Del Grosso, E.; Ragazzon, G.; Prins, L. J.; Ricci, F., Fuel‐responsive allosteric DNA‐based aptamers for the transient release of ATP and cocaine. *Angew. Chem., Int. Ed.* **2019,** *58* (17), 5582-5586.
26. Heinen, L.; Heuser, T.; Steinschulte, A.; Walther, A., Antagonistic Enzymes in a Biocatalytic pH Feedback System Program Autonomous DNA Hydrogel Life Cycles. *Nano Lett.* **2017,** *17* (8), 4989-4995.
27. Deng, J.; Bezold, D.; Jessen, H.; Walther, A., Multiple Light Control Mechanisms in ATP‐fueled Non‐Equilibrium DNA Systems. *Angew. Chem., Int. Ed.* **2020**.
28. Walther, A., From Responsive to Adaptive and Interactive Materials and Materials Systems: A Roadmap. *Advanced Materials* **2019**.
29. Zhao, Z.; Wang, C.; Yan, H.; Liu, Y., Soft Robotics Programmed with Double Crosslinking DNA Hydrogels. *Adv. Funct. Mater.* **2019,** *29* (45), 1905911.
30. Fern, J.; Schulman, R., Modular DNA strand-displacement controllers for directing material expansion. *Nat. Commun.* **2018,** *9* (1), 3766.
31. Zhang, Y.; Tu, J.; Wang, D.; Zhu, H.; Maity, S. K.; Qu, X.; Bogaert, B.; Pei, H.; Zhang, H., Programmable and Multifunctional DNA-Based Materials for Biomedical Applications. *Adv. Mater.* **2018,** *30* (24), 1703658.
32. Gačanin, J.; Synatschke, C. V.; Weil, T., Biomedical Applications of DNA‐Based Hydrogels. *Adv. Funct. Mater.* **2019,** *30* (4), 1906253.
33. Li, J.; Zheng, C.; Cansiz, S.; Wu, C.; Xu, J.; Cui, C.; Liu, Y.; Hou, W.; Wang, Y.; Zhang, L., Self-assembly of DNA nanohydrogels with controllable size and stimuli-responsive property for targeted gene regulation therapy. *J. Am. Chem. Soc.* **2015,** *137* (4), 1412-1415.
34. Wang, C.; Fischer, A.; Ehrlich, A.; Nahmias, Y.; Willner, I., Biocatalytic Reversible Control of the Stiffness of DNA-Modified Responsive Hydrogels: Applications as Shape-Memory, Self-Healing and Autonomous Controlled Release of Insulin. *Chem. Sci.* **2020,** *11*, 4516-4524.
35. Merindol, R.; Delechiave, G.; Heinen, L.; Catalani, L. H.; Walther, A., Modular Design of Programmable Mechanofluorescent DNA Hydrogels. *Nat. Commun.* **2019,** *10* (1), 528.
36. Ma, V. P. Y.; Salaita, K., DNA Nanotechnology as an Emerging Tool to Study Mechanotransduction in Living Systems. *Small* **2019,** *15* (26), 1900961.
37. Kishi, J. Y.; Schaus, T. E.; Gopalkrishnan, N.; Xuan, F.; Yin, P., Programmable autonomous synthesis of single-stranded DNA. *Nat. Chem.* **2017,** *10* (2), 155-164.
38. Palluk, S.; Arlow, D. H.; De Rond, T.; Barthel, S.; Kang, J. S.; Bector, R.; Baghdassarian, H. M.; Truong, A. N.; Kim, P. W.; Singh, A. K., De novo DNA synthesis using polymerase-nucleotide conjugates. *Nat. Biotechnol.* **2018,** *36* (7), 645.
39. Kosuri, S.; Church, G. M., Large-scale de novo DNA synthesis: technologies and applications. *Nat. Methods* **2014,** *11* (5), 499-507.
40. Wang, L.; Jiang, S.; Chen, C.; He, W.; Wu, X.; Wang, F.; Tong, T.; Zou, X.; Li, Z.; Luo, J., Synthetic genomics: from DNA synthesis to genome design. *Angew. Chem., Int. Ed.* **2018,** *57* (7), 1748-1756.
41. Lonnberg, H., Synthesis of oligonucleotides on a soluble support. *Beilstein J. Org. Chem.* **2017,** *13*, 1368-1387.
42. Molina, A. G.; Sanghvi, Y. S., Liquid‐Phase Oligonucleotide Synthesis: Past, Present, and Future Predictions. *Curr. Protoc. Nucleic Acid Chem.* **2019,** *77* (1), e82.
43. Bonora, G. M.; Scremin, C. L.; Colonna, F. P.; Garbesi, A., HELP (High Efficiency Liquid Phase) new oligonucleotide synthesis on soluble polymeric support. *Nucleic Acids Res.* **1990,** *18* (11), 3155-3159.
44. Bonora, G. M.; Biancotto, G.; Maffini, M.; Scremin, C. L., Large scale, liquid phase synthesis of oligonucleotides by the phosphoramidite approach. *Nucleic Acids Res.* **1993,** *21* (5), 1213-1217.
45. Molina, A. G.; Jabgunde, A. M.; Virta, P.; Lönnberg, H., Solution phase synthesis of short oligoribonucleotides on a precipitative tetrapodal support. *Beilstein J. Org. Chem.* **2014,** *10* (1), 2279-2285.
46. Matsuno, Y.; Shoji, T.; Kim, S.; Chiba, K., Synthetic Method for Oligonucleotide Block by Using Alkyl-Chain-Soluble Support. *Org. Lett.* **2016,** *18* (4), 800-803.

47. Kungurtsev, V.; Lönnberg, H.; Virta, P., Synthesis of protected 2′-O-deoxyribonucleotides on a precipitative soluble support: a useful procedure for the preparation of trimer phosphoramidites. *RSC Adv.* **2016,** *6* (107), 105428-105432.
48. Schwenger, A.; Birchall, N.; Richert, C., Solution‐Phase Synthesis of Branched Oligonucleotides with up to 32 Nucleotides and the Reversible Formation of Materials. *Eur. J. Org. Chem.* **2017,** *2017* (39), 5852-5864.
49. de Koning, M. C.; Ghisaidoobe, A. B.; Duynstee, H. I.; Ten Kortenaar, P. B.; Filippov, D. V.; van der Marel, G. A., Simple and efficient solution-phase synthesis of oligonucleotides using extractive work-up. *Org. Process Res. Dev.* **2006,** *10* (6), 1238-1245.
50. Gimenez Molina, A.; M Jabgunde, A.; Virta, P.; Lonnberg, H., Assembly of short oligoribonucleotides from commercially available building blocks on a tetrapodal soluble support. *Curr. Org. Synth.* **2015,** *12* (2), 202-207.
51. Kim, J. F.; Gaffney, P. R.; Valtcheva, I. B.; Williams, G.; Buswell, A. M.; Anson, M. S.; Livingston, A. G., Organic solvent nanofiltration (OSN): a new technology platform for liquid-phase oligonucleotide synthesis (LPOS). *Org. Process Res. Dev.* **2016,** *20* (8), 1439-1452.
52. Tanaka, S.; Wakabayashi, K.; Fukushima, K.; Yukami, S.; Maezawa, R.; Takeda, Y.; Tatsumi, K.; Ohya, Y.; Kuzuya, A., Intelligent, Biodegradable, and Self‐Healing Hydrogels Utilizing DNA Quadruplexes. *Chem. - Asian J.* **2017,** *12* (18), 2388-2392.
53. Tanaka, S.; Yukami, S.; Fukushima, K.; Wakabayashi, K.; Ohya, Y.; Kuzuya, A., Bulk pH-Responsive DNA Quadruplex Hydrogels Prepared by Liquid-Phase, Large-Scale DNA Synthesis. *ACS Macro Lett.* **2018,** *7* (3), 295-299.
54. Septak, M., Kinetic Studies on Depurination and Detritylation of CPG-Bound Intermediates During Oligonucleotide Synthesis. *Nucleic Acids Res.* **1996,** *24* (15), 3053-3058.
55. Lueckerath, T.; Strauch, T.; Koynov, K.; Barner-Kowollik, C.; Ng, D. Y.; Weil, T., DNA–Polymer Conjugates by Photoinduced RAFT Polymerization. *Biomacromolecules* **2018,** *20* (1), 212-221.
56. Liu, K.; Zheng, L.; Liu, Q.; de Vries, J. W.; Gerasimov, J. Y.; Herrmann, A., Nucleic acid chemistry in the organic phase: from functionalized oligonucleotides to DNA side chain polymers. *J. Am. Chem. Soc.* **2014,** *136* (40), 14255-62.
57. Wilks, T. R.; O'Reilly, R. K., Efficient DNA-Polymer Coupling in Organic Solvents: A Survey of Amide Coupling, Thiol-Ene and Tetrazine-Norbornene Chemistries Applied to Conjugation of Poly(N-Isopropylacrylamide). *Sci. Rep.* **2016,** *6*, 39192.
58. Madsen, M.; Gothelf, K. V., Chemistries for DNA Nanotechnology. *Chem. Rev.* **2019,** *119* (10), 6384-6458.
59. Schnitzler, T.; Herrmann, A., DNA Block Copolymers: Functional Materials for Nanoscience and Biomedicine. *Acc. Chem. Res.* **2012,** *45* (9), 1419–1430.
60. Creusen, G.; Roshanasan, A.; Garcia Lopez, J.; Peneva, K.; Walther, A., Bottom-up design of model network elastomers and hydrogels from precise star polymers. *Polym. Chem.* **2019,** *10* (27), 3740-3750.
61. Shibayama, M.; Li, X.; Sakai, T., Precision polymer network science with tetra-PEG gels—a decade history and future. *Colloid Polym. Sci.* **2018,** *297* (1), 1-12.
62. Parada, G.; Zhao, X., Ideal Reversible Polymer Networks. *Soft Matter* **2018,** *14* (25), 5186-5196.
63. Lin, T.-S.; Wang, R.; Johnson, J. A.; Olsen, B. D., Topological Structure of Networks Formed from Symmetric Four-Arm Precursors. *Macromolecules* **2018,** *51* (3), 1224-1231.
64. Tunn, I.; de Léon, A. S.; Blank, K. G.; Harrington, M. J., Tuning coiled coil stability with histidine-metal coordination. *Nanoscale* **2018,** *10* (48), 22725-22729.
65. Hörner, M.; Raute, K.; Hummel, B.; Madl, J.; Creusen, G.; Thomas, O. S.; Christen, E. H.; Hotz, N.; Gübeli, R. J.; Engesser, R., Phytochrome‐Based Extracellular Matrix with Reversibly Tunable Mechanical Properties. *Adv. Mater.* **2019,** *31* (12), 1806727.
66. Wu, J.; Li, P.; Dong, C.; Jiang, H.; Bin, X.; Gao, X.; Qin, M.; Wang, W.; Bin, C.; Cao, Y., Rationally designed synthetic protein hydrogels with predictable mechanical properties. *Nat. Commun.* **2018,** *9* (1), 620.
67. Anderson, A. J.; Culver, H. R.; Bryant, S. J.; Bowman, C. N., Viscoelastic and thermoreversible networks crosslinked by non-covalent interactions between “clickable” nucleic acid oligomers and DNA. *Polym. Chem.* **2020,** *11*, 2959-2968.
68. Gaffney, P. R.; Kim, J. F.; Valtcheva, I. B.; Williams, G. D.; Anson, M. S.; Buswell, A. M.; Livingston, A. G., Liquid‐Phase Synthesis of 2′‐Methyl‐RNA on a Homostar Support through Organic‐Solvent Nanofiltration. *Chem. - Eur. J.* **2015,** *21* (26), 9535-9543.

69. Bonora, G. M.; Rossin, R.; Zaramella, S.; Cole, D. L.; Eleuteri, A.; Ravikumar, V. T., A Liquid-Phase Process Suitable for Large-Scale Synthesis of Phosphorothioate Oligonucleotides. *Org. Process Res. Dev.* **2000,** *4* (3), 225-231.
70. Ravikumar, V. T.; Krotz, A. H.; Cole, D. L., Efficient synthesis of deoxyribonucleotide phosphorothioates by the use of DMT cation scavenger1. *Tetrahedron Lett.* **1995,** *36* (37), 6587-6590.
71. Suzuki, T.; Ohsumi, S.; Makino, K., Mechanistic studies on depurination and apurinic site chain breakage in oligodeoxyribonucleotides. *Nucleic Acids Res.* **1994,** *22* (23), 4997-5003.
72. Conrad, N.; Kennedy, T.; Fygenson, D. K.; Saleh, O. A., Increasing valence pushes DNA nanostar networks to the isostatic point. *Proc. Natl. Acad. Sci. U. S. A.* **2019,** *116* (15), 7238-7243.
73. Xing, Z.; Caciagli, A.; Cao, T.; Stoev, I.; Zupkauskas, M.; O'Neill, T.; Wenzel, T.; Lamboll, R.; Liu, D.; Eiser, E., Microrheology of DNA hydrogels. *Proc. Natl. Acad. Sci. U. S. A.* **2018,** *115* (32), 8137-8142.
74. Fernandez-Castanon, J.; Bianchi, S.; Saglimbeni, F.; Di Leonardo, R.; Sciortino, F., Microrheology of DNA hydrogel gelling and melting on cooling. *Soft Matter* **2018,** *14* (31), 6431-6438.